PALEONTOLOGY

Physiology and climate change explain unusually high similarity across marine communities after end-Permian mass extinction

Jood A. Al Aswad[1]*, Justin L. Penn[2], Pedro M. Monarrez[1,3], Mohamad Bazzi[1], Curtis Deutsch[2], Jonathan L. Payne[1]

Fossil assemblages exhibit a global depletion in taxonomic distinctiveness in the aftermath of the end-Permian mass extinction (~252 million years ago), but little is known about why. Here, we examine whether biotic homogenization can be explained by tropical survivors tracking an expansion of their preferred habitat, measured in terms of the ratio of environmental oxygen supply to metabolic demand. We compare spatial similarity in community composition among marine invertebrate fossils represented by bivalve and gastropod fossils with predictions from an ecophysiological model of habitat that diagnoses areas in the ocean that can sustain the aerobic requirements of marine invertebrates. Modeled biogeographic responses to climate change yield an increase in global similarity of community composition among surviving ecophysiotypes, consistent with patterns in the fossil record and arguing for a physiological control on earliest Triassic biogeography.

INTRODUCTION

The end-Permian extinction event caused a massive reduction in global biodiversity (*1*, *2*), and the ecosystems remaining in its immediate aftermath were often dominated by relatively few species [e.g., (*3*–*7*)]. Quantitative analysis of overall community composition for global terrestrial vertebrate (*8*, *9*) and marine invertebrate fossil assemblages (*10*, *11*) reveals a taxonomic homogenization of global ecosystems between the latest Permian Changhsingian stage and earliest Triassic Induan stage, but the underlying causes remain poorly understood. Potential explanations, which are not mutually exclusive, include (i) regionally heterogeneous signals, which can arise from either the low dispersion of fossil sites or the dominance of a region exhibiting unusually high compositional similarity; (ii) selective extinction of endemic taxa; (iii) expansion of physiologically preferred habitat for survivors; and (iv) ecological release of survivors from antagonistic or competitive interspecific relationships that limit biogeographic range [e.g., (*7*)].

Biotic homogenization (i.e., a reduction in β-diversity) has occurred several times in Earth's history [e.g., (*9*–*12*)], but the underlying mechanisms have yet to be explored (*13*, *14*). Here, we test a mechanistic basis for postextinction homogenization in the earliest Triassic using the fossil record of marine bivalves and gastropods. These classes are chosen for their relative abundance and diversity in the fossil record across the extinction event, which enables quantification of the effects of sampling, survivorship, and migration on measures of taxonomic similarity in marine communities across the end-Permian mass extinction. We compare fossil similarity patterns to community assemblages predicted from physiological constraints on marine animal habitats in Earth system model simulations of Permian/Triassic (P/Tr) climate change. The comparison provides a direct test of how much ecosystem homogenization can be explained by the aerobic habitat and thermal expansion of survivors as they track viable oceanographic niches (Fig. 1).

[1]Department of Earth and Planetary Sciences, Stanford University, 450 Jane Stanford Way, Stanford, CA 94305, USA. [2]Department of Geosciences, Princeton University, Guyot Hall, Princeton, NJ 08544, USA. [3]Department of Earth, Planetary, and Space Sciences, University of California, Los Angeles, CA 90095, USA.
*Corresponding author. Email: jalaswad@stanford.edu

RESULTS

Similarity decayed with distance

We compute three measures of similarity: (i) biogeographic connectedness (BC; see Materials and Methods) defined by the bipartite taxon-locality density measure [e.g., (*8*)]; (ii) the Jaccard coefficient; and (iii) quantified Czekanowski's coefficient [e.g., (*15*)]. For all metrics, similarity is measured on a scale from 0 (totally endemic, no taxa shared among grid cells) to 1 (globally homogenized, all taxa occur in all sampled grid cells) (*1*). Overall, the BC of well-sampled ($n \geq 20$ occurrences) cells increased from 0.25 in the Changhsingian to 0.63 in the Induan (fig. S1), consistent with patterns in terrestrial tetrapods (*9*), ammonoids (*10*, *11*), anthozoans (*11*), bryozoans (*11*), and bivalves (*11*, *12*).

When calculating the pairwise similarity of genus occurrences using the Jaccard index and Czekanowski's coefficient, we perform a set of subsampling procedures to reduce the potential effects of spatial and fossil sampling biases on the data (Fig. 2 and see Materials and Methods). Both the Jaccard and Czekanowski's coefficients exhibit the expected decrease in similarity with distance of compared cell pairs before the extinction (Fig. 2, A and B). From the Late Permian Changhsingian age to the earliest Triassic Induan age, both similarity measures increase substantially for cells separated by equivalent distances, and postextinction similarity remains high regardless of cell area (fig. S2) and distance between cell pairs (Fig. 2, A and B). Taxonomic homogenization in the earliest Triassic is reflected by an increase in similarity at any given distance and a reduction in the decay of similarity with distance. Thus, the Changhsingian-to-Induan increase in BC is not explained by changes in the spatial distribution of fossil data. Homogenization occurs independently when cells are subset to only tropical latitudes (0° to 30° North and South), only extratropical latitudes (30° to 90° North and South), and the Northern, Southern, Eastern, and Western hemispheres (figs. S3 to S5).

Endemic extinction and survivor expansion

One potential driver for the observed Induan homogenization is the preferential extinction of narrowly ranging taxa (*15*). To determine the degree to which increases in similarity resulted simply from the selective extinction of genera with narrower ranges (i.e., via selective

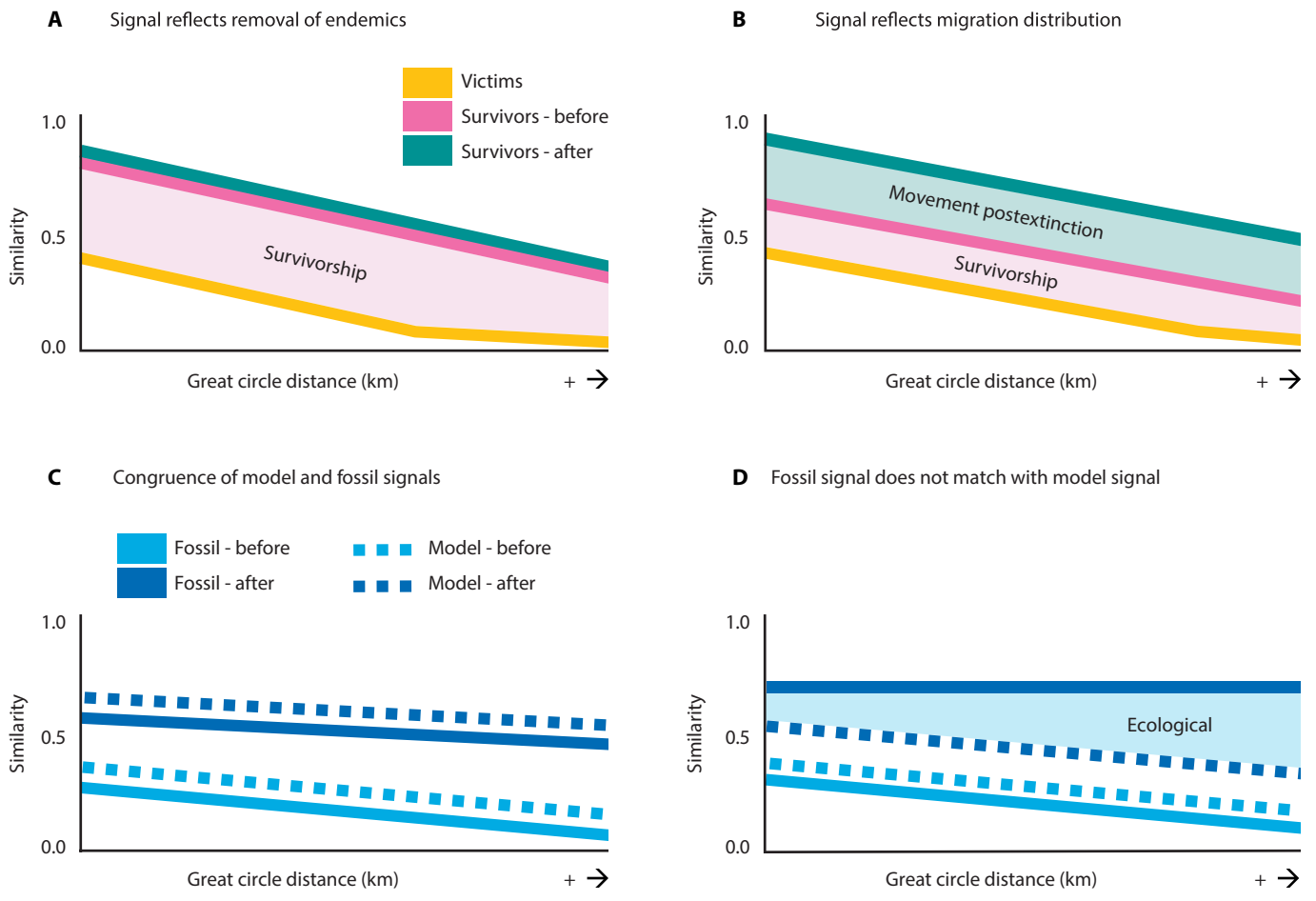

Fig. 1. Conceptual framework for investigating causes of postextinction homogenization. (**A** and **B**) The feasibility of the hypothesis regarding the removal of victims (yellow line), which were more narrowly ranging than survivors (pink line), is investigated. If the homogenization signal is fully explained by a difference in the similarity between communities of survivors and victims, then the similarity signal of survivors would not change postextinction [pink and green lines in (A)]. However, if the homogenization signal is only partially explained by the removal of endemic victims, then an increase in the similarity of survivor occurrences after the extinction event [green line in (B)] would indicate that further scenarios for postextinction homogenization are required to explain the increase similarity. (**C** and **D**) The similarity signals of the fossil genus occurrences (solid lines) are compared to those of the model ecophysiotype occurrences (dashed lines). If the fossil and model signals are congruent with one another (C), then the postextinction homogenization can be explained via environmental factors. However, if the model similarity differs from the fossil similarity in the postextinction interval (D), then the signal is likely to be more strongly influenced by ecological factors.

loss of genera with narrow ranges rather than via geographic expansion of survivors), we calculated similarity separately for victims and survivors in the Changhsingian fossil record (see Materials and Methods). At any given distance, surviving genera alone exhibit greater similarity than victims before extinction, and both groups exhibit decreasing similarity with distance (Fig. 2, C and D). The similarity of the survivors at any given distance during the Changhsingian is substantially lower than the similarity of the same taxa during the Induan. The removal of extinction victims is, therefore, not sufficient, on its own, to explain the taxonomic homogenization of the marine ecosystems and accounts for only a minority of the overall change. Thus, biogeographic expansion is required to account for most of the biotic homogenization following the end-Permian extinction.

Environmental tolerance propelled homogenization

To test whether the expansion of the physiologically preferred habitats of survivors can explain observed ecosystem homogenization, we simulate patterns of end-Permian extinction and earliest Triassic survivorship. The simulations combine a trait-based ecophysiological model of animal habitat and Earth system model simulations of the P/Tr climate transition, previously shown to explain biogeographic selectivity of extinction (*16*). We equilibrated the initial climate under end-Permian paleogeography and then forced a sustained rise in atmospheric CO_2 to induce the magnitudes of climate warming and ocean O_2 loss into the earliest Triassic implied by proxy reconstructions (*17*, *18*). The effects of warming and O_2 loss on ocean habitat for water-breathing animals are accounted for by the ratio of temperature (T)–dependent O_2 supply to demand rates (Φ), which vary as a function of species-specific physiological traits (i.e., hypoxia tolerance and its temperature sensitivity) and ocean conditions [T and oxygen partial pressure (pO_2)] (see Materials and Methods). Aerobic habitat is available wherever ocean conditions allow the O_2 supply-to-demand ratio to exceed the species-specific minimum threshold required to sustain a viable population (Φ_{crit}). At species' cold edges, the aerobic habitat niche is limited by minimum tolerances to T (*19*), as diagnosed from biogeographic and

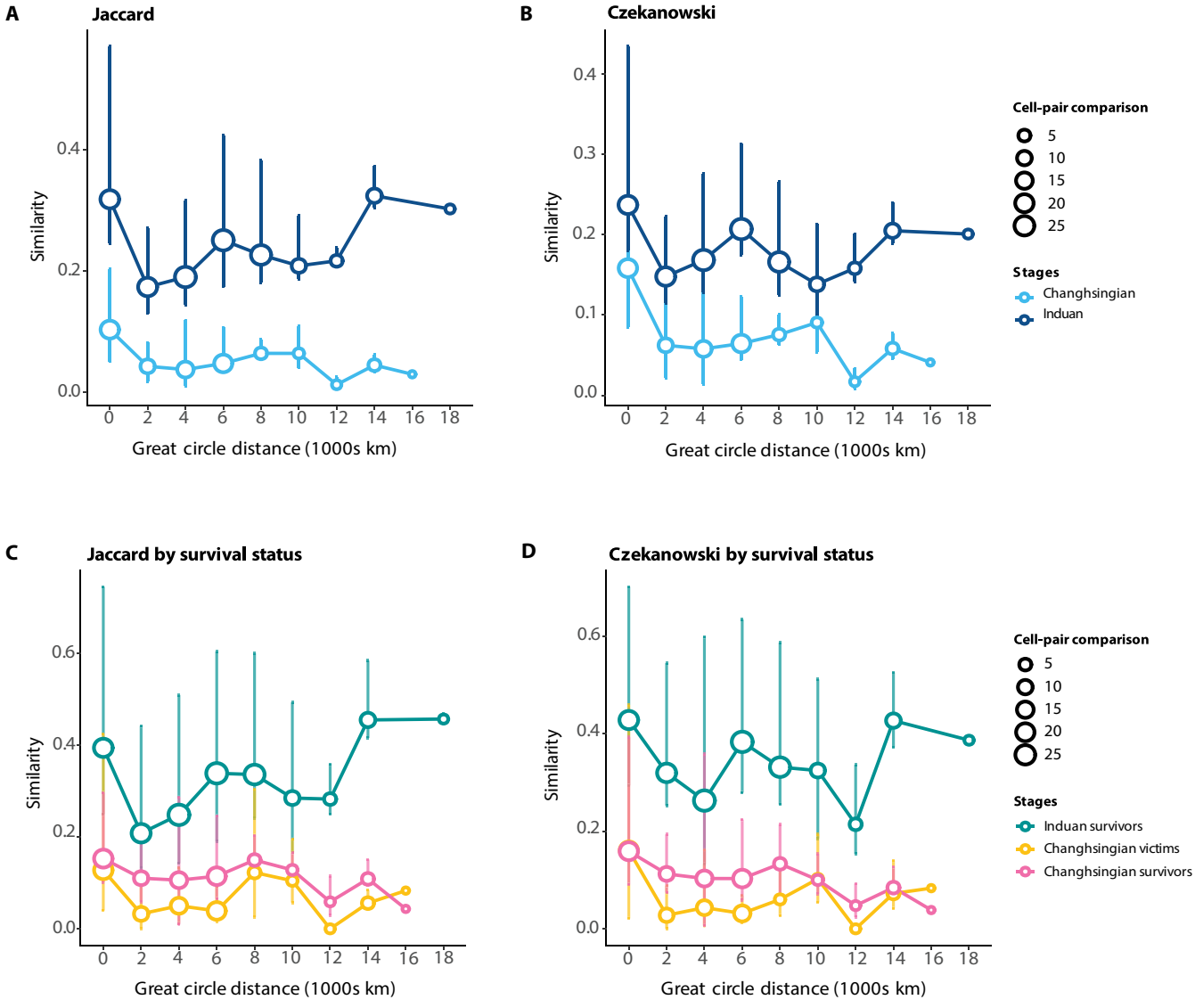

Fig. 2. Mean taxonomic similarity for the late Permian Changhsingian and Early Triassic Induan age. For each cell, 20 occurrences were randomly subsampled without replacement 1000 times. Vertical bars represent the 2.5 and 97.5% error bars of the middle 95% of the samples. (**A** and **B**) Compositional similarity of the total population. (**C** and **D**) Compositional similarity of occurrences based on survival status. Induan mean similarity is higher than the Changhsingian signal across all distances. For all Changhsingian trends, mean similarity decays with distance. Distances between cells for pairwise comparisons are in thousands of kilometers. Bubbles represent the number of cell-pair comparisons for each distance interval.

climate data (*20*). Model taxa (hereafter ecophysiotypes, treated as equivalent to genera for purposes of model-data comparison) are determined by the frequency of observed species with a given set of traits, derived from respirometry experiments and biogeographic data of diverse living biota, including bivalves and gastropods (*21*).

Model biogeography is predicted from physiological traits and environmental conditions but is not constrained to match species distribution data in either modern or paleoclimate intervals. Any correspondence between observations and model predictions of biogeographic and biodiversity patterns, thus, supports the fundamental premise that aerobic conditions are a central driver of community assembly. Model richness patterns reproduce the observed latitudinal diversity gradient in the modern ocean (*20*), including the equatorial dip in species richness caused by warm, low-O_2 conditions that exceed species' tolerances, indicating that the model captures key aspects of marine biogeography and the decrease in oxygen in warmer waters due to the reduction in solubility.

Modern species' traits are hypothesized to be largely representative of end-Permian groups due to the similarity of initial climate states (T and pO_2). Model simulations indicate that all regions of the end-Permian ocean conditions are inhabited, and the vast majority of modern ecophysiotypes finds habitat somewhere in the ocean, which is consistent with the Changhsingian fossil record and indicates that modern species are well adapted to end-Permian conditions (*16*).

Ocean warming increases the metabolic demand for O_2 while lowering the ocean's O_2 content. Aerobic habitat is lost wherever the local O_2 supply falls below the physiological demand for a species,

leading to species' extirpation (*22*). If enough habitat is lost globally, then any remaining habitat may no longer sustain a viable population, leading to extinction on the timescales considered here (more than thousands of years). Global extinction occurs in the model when relative habitat loss exceeds a critical fraction (here 50%), calibrated by comparison of the model extinction magnitudes to the end-Permian fossil record (*16*, *20*). The geographic selectivity of extinction, with increased losses at higher latitudes, is consistent with results from prior studies of the thermal and latitudinal selectivity of marine invertebrate extinction from the end-Permian fossil record (*10*, *16*, *23*–*25*). Although the taxonomic groupings and analytical methods vary across these studies, all studies find evidence for preferential extinction of benthic invertebrate genera in higher latitudes. The statistical significance of this pattern remains ambiguous and may depend on the treatment of genera from the basal Triassic "mixed" faunas that survived for a short time beyond the major extinction pulse (*24*). Here, we also simulate the biogeographic and richness distributions of survivors that colonize newly available habitat in the warm, low-O_2 Triassic wherever climate conditions fall within physiological tolerances (Fig. 3).

We analyze similarity changes in the pre- and postextinction communities of model ecophysiotypes using the Jaccard coefficient that is also applied to the fossil record (see Materials and Methods). Consistent with fossil data, ecosystem similarity between two sites in the model decreases as the distance between them increases, especially before the extinction event (Fig. 4). Model simulations predict an increase in similarity postextinction, with greater changes at further distances, qualitatively consistent with the patterns observed in fossil data (Fig. 4). This pattern of initial similarity and its change is found in the entire upper ocean, global shelf regions, and at the sampling locations of the fossil record (fig. S6).

However, absolute values of similarity are higher in the model than in the fossil record. This difference may arise because ecophysiotypes exhibit wider geographic ranges, on average, than genera. It could also arise because the similarity analysis performed in the model assumes a world in which all organisms are preserved and sampled everywhere. We assess the potential influence of sampling on differences in absolute similarity in the model versus in the fossil record by assuming that only a random fraction of ecophysiotypes leaves a fossil at each location in the model. In this case, we find that absolute values of similarity in the model decrease. This decrease occurs because even if a taxon is present in multiple locations, it will not necessarily be sampled in all of them, decreasing the calculated similarity index. We find that a value of 40% for the sampled fraction reasonably reproduces the initial absolute values of similarity from the fossil data, while preserving the similarity increase across the extinction event. A comparable pattern of similarity change occurs if the model is randomly sampled only at the paleo-coordinates of fossil locations, indicating that fossil data are well enough dispersed to sample a global signal, but doing so introduces noise in the relationship between similarity and distance, which is also evident in the fossil data (fig. S7).

Ecosystem homogenization arises in the model simulations due to the expanding physiological niches and associated geographic

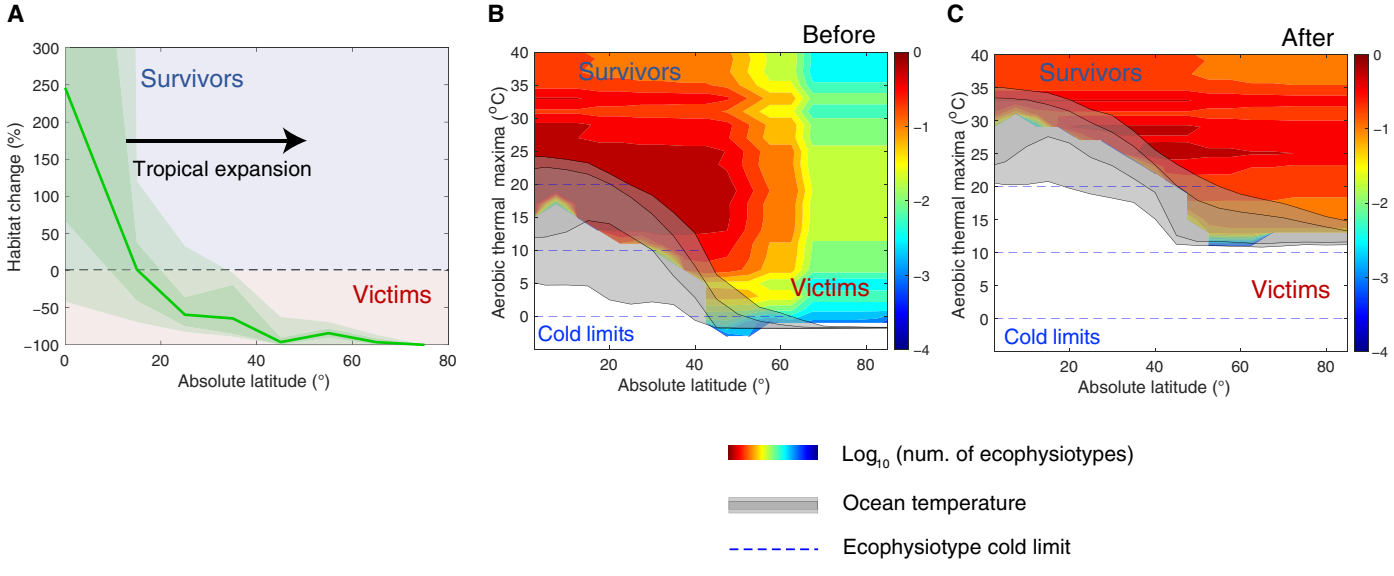

Fig. 3. Mechanism of ecosystem homogenization. (**A**) Tropical habitat expands at the expense of the extratropics. In (A), the line (shading) shows the median relative habitat volume changes across ecophysiotypes. Outer and inner shaded regions show the 1 to 99 and 16 to 84 percentiles, respectively. (**B** and **C**) Tropical ecophysiotypes preferentially survive by having traits able to withstand warm, low O_2 conditions (measured by a high aerobic thermal maximum, AT_{max}^{act}) and experience habitat growth as poleward ocean temperatures rise above cold limits (illustrated by dashed blue lines, which show maximum poleward extent of habitat for a given minimum *T* threshold). The resulting biotic homogenization can be seen in the more uniform distribution of ecophysiotypes versus latitude postextinction (colors). In contrast to survivors, extinction victims have traits adapted to cool, high O_2 climate conditions (low AT_{max}^{act}), which disappear under climate warming. In (B) and (C), colors show the number of ecophysiotypes (log_{10}) with a given AT_{max}^{act} at a given absolute latitude, normalized to the maximum number of ecophysiotypes locally present before extinction so that the most bio-rich regions take a value of 1 and depauperate regions approach 0. Decreases (increases) in the number of ecophysiotypes can arise from extinctions and extirpations (colonizations). Species with aerobic thermal maxima below ocean temperatures [0 to 200 m; gray shading; same percentiles as in (A)] are excluded (white region). Aerobic thermal maximum (AT_{max}^{act}) is the upper *T* threshold for active aerobic metabolism (i.e., where $\Phi = \Phi_{crit}$) at a given p_{O_2} (here, 0.209 atm) and effectively incorporates all species-specific physiological traits of the metabolic index into a single metric (*21*).

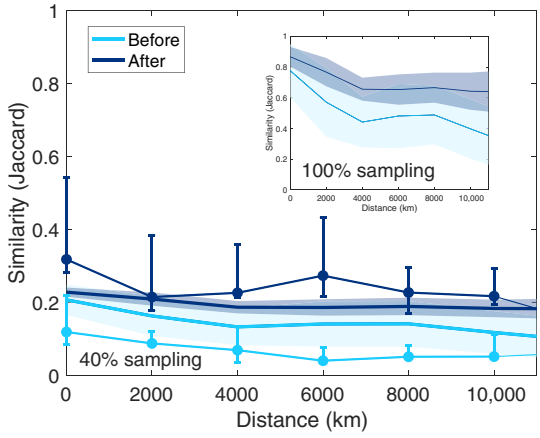

Fig. 4. Ecosystem homogenization in climate-ecophysiological model simulations. Thick lines show average model relationships between taxonomic similarity and distance, and shading shows the SD in this relationship across ocean regions. Fossil record observations are shown as points and thin lines (mean) with error bars (SD) (data from Fig. 2B). Model simulations show decline in compositional similarity of marine ecosystems with distance and a postextinction increase across the oceanic shelf. With complete (100%) sampling of the model, the magnitude of initial similarity is higher than in the fossil record (inset). The initial observed similarity versus distance relationship and its postextinction change is reproduced when accounting for incomplete sampling by the fossil record, assuming that a random selection of 40% of all ecophysiotypes leaves a fossil at a given location (lower set of curves).

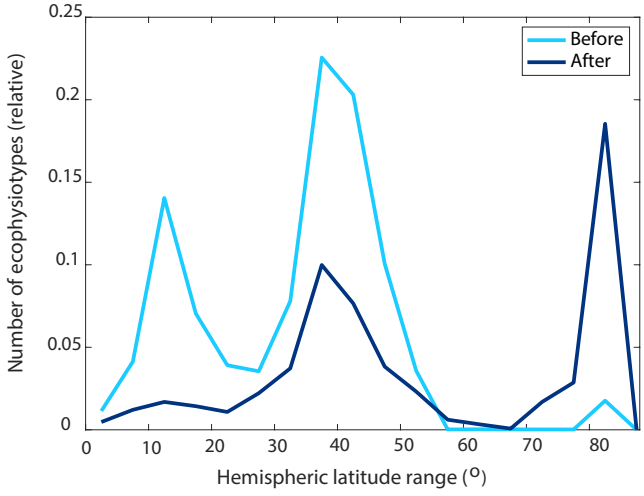

Fig. 5. Simulated latitude range expansion of extinction survivors. Histograms of ecophysiotype range size (degrees latitude) show an increase for survivors (dark blue) compared to victims and survivors before extinction (light blue), consistent with the simulated and observed similarity change. Notably, there is a large uptick in the fraction of cosmopolitan species postextinction. Latitude range size is computed as the difference between 95th and 5th percentile of inhabited absolute latitude for each ecophysiotype. The number of ecophysiotypes (y-axis) is normalized to the global number of initial ecophysiotypes before extinction.

range sizes of tropical survivors and the disproportionate loss of endemic extratropical victims (Figs. 3A and 4). Before the extinction, the high hypoxia tolerance and weak temperature sensitivity traits of tropical ecophysiotypes confer them with upper temperature limits for aerobic metabolism, termed aerobic thermal maxima (*21*), allowing them to withstand the heat of tropical waters (Fig. 3B). By contrast, extratropical ecophysiotypes require lower ocean temperatures to sustain aerobic metabolism. Extreme climate warming removes this cool-water niche globally, leading to preferential extinction in the high latitudes (*16*, *23*), while tropical ecophysiotypes can survive under these conditions and respond to habitat expansion via poleward colonization as ocean temperatures rise above species cold limits (Fig. 3C). The resulting range expansions lead to a more uniform geographic distribution of survivors (Fig. 5) and explain the model ecosystem homogenization signal (Fig. 4). The model predictions are broadly consistent with observations of a flattened latitudinal diversity gradient in the Early Triassic (*26*). The correspondence between model simulations and fossil observations supports the hypothesis that the postextinction homogenization was driven by environmental niche expansion, approximated here by considering only the roles of temperature and oxygen in determining metabolically viable habitat.

DISCUSSION

The earliest Triassic fossil record of bivalves and gastropods exhibits unusual spatial homogeneity, consistent with data from other taxa [e.g., (*8*–*10*)]. Subsampled measures of similarity with respect to distance indicate that the overall global increase in taxonomic similarity is not due to data coming from more closely spaced sample sites during the Induan or to spatiotemporal sampling bias (Fig. 2 and figs. S2 to S5 and S8). In addition, analyses separating survivors from victims during the Changhsingian (latest Permian) demonstrate that only a small fraction of the increase in similarity can be explained by the fact that victims tended to have narrower geographic distributions than survivors [e.g., (*8*, *10*)] (Fig. 2, C and D). Although we cannot entirely rule out the survival of any specific "victim" genus due to sampling gaps, the absence of numerous temperate genera sampled in the Changhsingian from not only the Induan but also the later Triassic fossil record indicates that they were true extinction victims. Furthermore, given the spatial and temporal scale of this study and the generally thorough sampling of bivalves and gastropods at the genus level (*27*, *28*), we interpret that the likelihood of survival for these genera appears low.

Several lines of evidence demonstrate that habitat tracking is sufficient to account for postextinction taxonomic homogenization of marine ecosystems. First, on their own, fossil data are compatible with survivors tracking the expansion of their preferred habitat niches as the primary explanation for taxonomic homogenization. Second, homogenization is predicted by the mechanistic ecophysiological simulations in an Earth system model due to the expansion of warm, low-oxygen conditions and is consistent with the pattern seen in the fossil record (Figs. 3 and 4). If, instead, the model response indicated little or no biogeographic change in ecophysiotypes based on physiological preferences, then the pattern of homogenization observed in the fossil record would require ecological processes, such as release from constraints imposed by antagonists and competitors. Third, the extinction pattern itself is consistent with an important role for temperature-dependent hypoxia in driving the loss of habitat and genera (*16*). Fourth, temperature and oxygen are skillful predictors of geographic distribution for the extant, benthic marine fauna (*14*, *29*, *30*).

Other potential kill mechanisms, such as acidification and hypercapnia, may still be required to explain patterns of taxonomic

selectivity and may enhance biogeographic predictions, but quantitative, predictive physiological models incorporating these mechanisms are not yet available. Although the metabolic index used in this study does not account for the additional potential effects of pH, salinity, sulfide, carbonate saturation state, and other factors that often interact with one another, T and pO_2, nevertheless, predict the basic biogeographic structure observed in the fossil record and account for the geographic selectivity of extinction, consistent with the ability of temperature-dependent hypoxia to account for habitat range limits of diverse species in the modern ocean (*21*, *29*, *31*). To that end and given the timescale of this study, we assume that a genus maintains its ecological and physiological preferences after the extinction event. This simplifying assumption of invariance in physiological and ecological preferences is undoubtedly imperfect but is consistent with the fact that physiological and ecological differences within genera tend to be much smaller than differences among genera and, therefore, any changes that did occur through the study interval would be unlikely to qualitatively alter our interpretations.

Implications for interpreting "disaster" taxa

Congruence between the fossil analysis on taxonomic homogenization and the modeled biogeography of ecophysiotypes in this study suggests that disaster taxa that are abundant in certain Early Triassic fossil assemblages, such as the bivalve *Claraia*, lingulid brachiopods, and the foraminifera *Earlandia* and *Postcladella*, reflect a response to abiotic rather than biotic conditions (*4*, *32*, *33*). For example, the selective survival and subsequent dominance of three bivalve genera (*Unionites*, *Eumorphotis*, and *Promyalina*) have been hypothesized in previous studies to result from the physiological advantages of bivalves over rhynchonelliform brachiopods, which include faster metabolism, more streamlined energy capture via feeding, and their ability to cope with stressful environmental conditions (*34*–*36*). The results of our study add support for these hypotheses and highlight the role of physiology in their selective extinction and recovery from the end-Permian mass extinction through the homogenization of ecophysiotypes more inured to the conditions of the earliest Triassic (Figs. 3 and 4), as well as the prevalence of disaster taxa in our Induan fossil dataset, which includes abundant and widespread occurrences of the *Claraia*, *Unionites*, *Eumorphotis*, and *Promyalina* genera (fig. S9).

Some of these disaster taxa, such as *Unionites* and *Claraia*, may be polyphyletic form genera, raising questions about whether they create the increase in similarity through inaccurate taxonomy rather than genuine change in biogeography. For the inclusion of polyphyletic form genera in the analysis to cause the observed change in biogeography, the Early Triassic requires a more pronounced form-genus problem than the Late Permian. Even if form genera are a bigger problem for the Early Triassic fossil record than for the Late Permian, a conservative approach of removing these taxa from the dataset entirely does not result in any discernible change in the overall result (fig. S10), and the same is true for problematic taxa defined by the total number of genus occurrences, following the criteria in (*37*) (figs. S11 and S12). Therefore, we interpret the change in biogeography across the Permian-Triassic transition as a primarily biological signature in the fossil record, not the product of poor taxonomic identifications.

We argue that ecophysiotypes that were well adapted to the oceanic conditions of the Early Triassic thrived in a world replete with warm, low-oxygen environments that allowed them to proliferate. The decline in these widely distributed taxa during the Middle Triassic (*4*) could also be attributed to the link between taxonomic homogeneity, animal physiology, and the ocean conditions of the Early Triassic: As an extreme climate ameliorated during the later Early Triassic and Middle Triassic (*26*), the warm, low-oxygen aerobic niches of the disaster taxa may have become spatially restricted.

Implications for rate and pattern of taxonomic diversification/recovery

The environmentally controlled taxonomic homogeneity of the earliest Triassic oceans raises questions about its effect on the pattern and timing of recovery. An unanswered question remains regarding the extent to which the slow increases in taxonomic diversity (*8*, *38*) and ecological complexity (*39*, *40*) result from environmental limitation by factors such as dysoxia and global warmth (*1*, *41*–*43*), Early Triassic environmental crises that interrupted recovery (*43*, *44*), or the limited starting diversity and complexity of Triassic ecosystems (*23*, *45*, *46*). Body evolution across taxonomic classes may be particularly informative (*47*, *48*). At broad temporal and taxonomic scales, maximum size decreased more than expected as a simple consequence of diversity loss in many benthic classes (*48*). Within the Early Triassic, however, there is evidence of size trends toward larger sizes within and among lineages in foraminifera (*49*, *50*), bivalves [e.g., (*51*)], gastropods (*52*, *53*), and ammonites (*48*). The extent to which these overall size trends relate to spatial gradients under environmental conditions remains little explored, although there is emerging evidence from bivalves that larger specimens and species preferentially occur in cooler and, perhaps, better oxygenated settings. The occurrences of Early Triassic radiolarians and hexactinellids in cooler, higher-latitude settings (*54*) further point toward physical and chemical control on Early Triassic paleobiogeography.

Application of the metabolic index to earliest Triassic oceanography and biogeography shows that these explanations need not be mutually exclusive. The broad distribution of warm, low-oxygen habitats could have limited recovery processes by creating ecosystems that supported low diversity and abundance (*55*) of taxa with a limited range of physiological and ecological traits (*56*, *57*), thereby reducing the role of both biogeographic and ecological factors that enable diversification.

The current biodiversity crisis is anticipated to herald changes in ecosystem composition that surpass even those seen in the earliest Triassic, which has been the greatest homogenization event to date (*58*, *59*). If our interpretation is correct, then it suggests that homogenization in the Anthropocene, enhanced beyond physiological controls by human-mediated biotic interchange, could play a role in delaying recovery of the biosphere beyond what might be predicted due to taxonomic losses alone.

MATERIALS AND METHODS

Experimental design

Fossil data

We downloaded and gridded global fossil occurrence data for marine bivalves and gastropod genera spanning the Changhsingian (latest Permian; ~254.2 to ~252.2 Ma) and Induan (earliest Triassic; ~251.9 to ~251.2 Ma) stages from the Paleobiology Database on 19 February 2024, yielding 1591 Permian and 2527 Triassic occurrences. These ages represent the immediate pre- and postextinction time intervals for the end-Permian mass extinction event. We chose these taxonomic classes for this study based on their rich stratigraphic

records across the Phanerozoic and their relatively high occurrence frequencies in both Changhsingian and Induan marine strata. We excluded genus occurrences noted with "aff.," "cf.," "ex gr.," "informal," "sensu lato," "?," and quotation marks. We elevated subgenera to genus rank for analysis. We excluded data with no paleogeographic location information and filtered the data for paleogeographic and taxonomic inconsistencies or invalid coordinates using the R packages *CoordinateCleaner* and *fossilbrush*, respectively (*60*, *61*). All codes are available at zenodo.org/doi/10.5281/zenodo.11522106.

Survival status

We discerned potential differences in similarity between the survivors and victims by dividing genus occurrences by their survival status. We first used Phanerozoic-level data from the Paleobiology Database to find the First Appearance Datum and Last Appearance Datum for each genus before subsetting the data to the Changhsingian and Induan stages. We then labeled genera with a Last Appearance Datum at the end of the Changhsingian as victims, whereas occurrences of genera that survived the Permian-Triassic transition (i.e., had first occurrences in the Changhsingian or earlier and last occurrences in the Induan or later) were labeled as survivors. To assess the extent to which the removal of endemic victims can explain postextinction homogenization, we compared the biogeography of survivors between the Changhsingian and Induan: If there was little difference between the similarity of survivors before and after the extinction event, then the removal of endemics is sufficient on its own to explain the Induan homogeneity. However, if there was a marked change in their similarity postextinction, then other processes must be investigated to explain that difference.

Equal-area hexagonal cells

We binned paleogeographic coordinates of all occurrences into a global grid of equal area icosahedral hexagonal cells using the *icosa* package on R (*62*) (fig. S13). We used a grid of 812 equal-area (629,000 km^2) cells instead of latitude-by-longitude grids to preserve area regardless of paleolatitude. To examine whether the similarity signal is affected by cell size resolution or number of cells used in cell-pair comparisons, we calculated and compared the similarity of cells with two different cell area resolutions, resulting in grids with 162 cells (3,146,947-km^2 cell area) and 4002 cells (127,238-km^2 cell area) to the resolution used in this study (fig. S2). Regardless of the cell area used, the signal of increased postextinction homogeneity is observable, indicating that the signal is independent of scaling the area of the localities used to calculate compositional similarity. We generated shapefiles supplied by Scotese (*63*) for Permian-Triassic global paleogeography using rotation files on the GPlates 2.0.0 software (*64*) and visualized using the *rgplates* package in R (*65*).

Model simulations

To test the role of physiology in explaining the similarity changes observed in the fossil record, we simulated the distributions of viable animal habitat in the ocean using an ecophysiological model and climate model simulations of the P/Tr transition (*16*, *20*, *21*). Briefly, we used previous climate and marine ecosystem model simulations from the Community Earth System Model run under end-Permian paleogeography and astronomical forcing. The initial climate state was equilibrated under low atmospheric CO_2 levels and then forced with an instantaneous and sustained increase in CO_2 to induce climate warming and ocean O_2 loss. Initial and perturbed climate states reproduce geochemical proxies for ocean temperature and anoxia (*17*, *18*, *40*). Climate model simulations and comparisons with proxy data are documented in detail in (*16*).

Statistical analysis

Fossil similarity assessment

We conducted the assessment of occurrence similarity patterns in equal-area hexagonal cells using the following measures: BC, the quantified Czekanowski's coefficient (also known as proportional similarity), and the Jaccard index. For all measures, similarity was quantified in a scale from 0 (totally endemic) to 1 (globally homogenized). BC, a bipartite density measure, calculates the global connectedness of the cells at a given time interval, and is written as

$$BC = \frac{(O-N)}{(CN-N)}$$

where O represents the number of occurrences of each genus in each cell, N is the total number of genera, and C is the number of cells (*14*). The numerator represents the number of occurrences of genera minus one occurrence for each genus so that the numerator would be zero if each genus occurred in only one cell and the denominator is the number of occurrences that could possibly occur (CN), minus one occurrence for each genus because each genus must occur at least once, allowing BC to reach unity if all genera occur in all cells.

BC is the simplest measure for biotic similarity that, in this study, provides an approximation of potential changes in similarity from the Changhsingian to the Induan. However, BC is not sufficient on its own to estimate biogeographic structure because it provides a single value for the total global similarity of all genera that occur in more than one cell and because the BC can produce the same value if genera share equivalent geographic range distributions but have varying biogeographic structures.

To complement the BC method, we measured similarity as a function of distance using the Jaccard index (*15*), which is based on the presence and absence of genus occurrences

$$J = \frac{m}{(m+a+b)}$$

where m is the number of genera present in both cells, a is the number of genera uniquely present in the first cell that is compared, and b is the number of genera that is uniquely present in the other cell.

The quantified Czekanowski's coefficient (*15*) is a pairwise comparison that is sensitive to variations in the number of genus occurrences in each cell. In this study, similarity values are cast as proportional values (multiplying by 100 would yield percent similarities)

$$C = 2\sum \min \frac{(x_{1k}, x_{2k})}{\left(\sum x_{1k} + \sum x_{2k}\right)}$$

where x_{1k} is the number of occurrences of the kth genus in the first cell that is compared and x_{2k} is the number of occurrences in the kth genus in the other cell.

We analyzed results from the quantified Czekanowski's coefficient alongside those from the Jaccard index method to assess different aspects of the change in biogeography. The Jaccard metric gives equal weight to common and rare taxa and, thus, only measures similarity of taxa present. Czekanowski's coefficient incorporates a measure of abundance (occurrence frequency, in this case) and can, therefore, provide further information regarding the extent to which commonness or rarity of taxa is shared across sites. Increases in both measures are, therefore, even greater indications of greater community similarity than an increase in either one or the other.

For all pairwise comparisons of occurrences, we conducted analyses on subsamples of cells and occurrences to correct for any differences in similarity resulting from differences in sampling completeness rather than biological variation. The following subsampling procedures have been conducted for each of the Jaccard index and Czekanowski's coefficient measurements: In each of 1000 iterations, we selected 13 cells without replacement from the Induan set to match the 13 cells available for the Changhsingian. For each cell, we then subsampled (without replacement) the number of occurrences down to 20 to ensure that sample size was uniform across cells (fig. S14). We then calculated similarity measures for each of these 1000 iterations. For each distance bin of the Jaccard and Czekanowski's coefficient measures, the average pairwise similarity of the 1000 subsampled iterations is calculated (Fig. 2).

In a separate analysis, along with the above subsampling procedures, we randomized occurrences with respect to cell to assess the null expectation under the condition that there is no biogeographic variation with respect to distance. Differences from this null expectation are required to indicate biogeographic structure in the data (fig. S7).

Separating the analysis by taxonomic class is not possible because the number of occurrences and dispersion of cells for gastropod data are not sufficient enough to carry out the analysis on their own. Bivalves have sufficient data to analyze on their own, and results of the bivalve-only analysis do not alter any of the conclusions derived from the combined analysis (fig. S15). To examine the impact of taxonomic reassignments and to mitigate errors associated with species reassignments within a genus, we also conducted the analysis using occurrences originally identified to species level (fig. S16).

Model taxa similarity

We computed the Jaccard similarity (J) of the simulated marine ecosystem before and after climate warming, ocean O_2 loss, and extinction by comparing communities of ecophysiotypes among model grid cells. It is not possible to apply the Czekanowski's coefficient to the model output, since the metabolic index addresses only presence (habitable) versus absence (not habitable), rather than population size. For comparison with fossil record analyses, we restricted similarity analyses to locations with bottom water depths shallower or equal to 200 m, equivalent to the model shelf regions where most fossils are found. We note that similarity changes in shelf regions are largely representative of the simulated changes for all ocean regions above 200 m, including the open ocean (fig. S6). We converted the three-dimensional occurrences (latitude, longitude, and depth) of model ecophysiotypes to two dimensional occurrences (latitude and longitude) above the shelf depth for comparison to the fossil analyses. We computed similarity by comparing the composition of ecophysiotypes in each grid cell to that in all other grid cells. To analyze similarity as a function of distance, we computed distances between each grid cell and all other grid cells using the MATLAB function *Distance.m*. For each grid cell, we computed similarity versus distance relationships between that grid cell and other cells by averaging similarity into 2000-km-distance bins chosen to match the binning scheme of the fossil analysis. We constructed global mean and variance in similarity versus distance relationships by averaging these relationships across model grid cells (lines in Fig. 4, inset) and taking their SD (shading in Fig. 4, inset).

The effects of ocean warming and O_2 loss on viable habitat for water-breathing animals are accounted for by the ratio of temperature (T)–dependent O_2 supply to demand rates (Φ), which vary as a function of ocean conditions (T and pO_2) and species-specific physiological traits, including resting hypoxia tolerance (A_o, 1/atm) and its temperature dependence, described by the Arrhenius exponential factor with temperature sensitivity trait, E_o (in electron volts), Boltzmann constant, k_B, and reference temperature, T_{ref} (here 15°C) (*21, 29, 31*)

$$\Phi = A_o pO_2 exp\left[\frac{E_o}{k_B}\left(\frac{1}{T}-\frac{1}{T_{ref}}\right)\right]$$

Aerobic habitat is available in the ocean wherever the O_2 supply to demand ratio (Φ) exceeds the species-specific energetic limit required to sustain active aerobic metabolism (Φ_{crit}) (*21*, *29*–*31*). At species' cold edges, the habitat niche is limited by minimum tolerances to temperature (T_{cold}) (*19*, *20*). We defined a set of model taxa ("ecophysiotypes") that vary in terms of their physiological traits (A_o, E_o, Φ_{crit}, and T_{cold}) and find habitat in the simulated ocean wherever $\Phi > \Phi_{crit}$ and $T > T_{cold}$. The number of unique ecophysiotypes in each grid cell depends on the number of trait combinations that find habitat in that location scaled by the observed frequency of species with that set of traits. We estimated metabolic index traits from respirometry experiments of diverse living biota (A_o and E_o) and biogeographic occurrence data paired with climatological observations of ocean T and O_2 (Φ_{crit}) (*20*, *21*). We estimated the distribution of T_{cold} as the lower 10th percentile of inhabited temperature from the paired occurrence climate data for 14,949 species (*20*). Under P/Tr climate change, model ecophysiotypes are allowed to colonize emerging habitat regions that exist wherever Φ rises above Φ_{crit} and T rises above T_{cold}. Across the climate transition, extinction of model ecophysiotypes occurred if the relative loss of global habitat volume (in cubic meters) in the upper ocean (0 to 500 m) exceeded a critical threshold required to sustain a population (here, 50%), calibrated from prior comparison of the model to the fossil record (*16*, *20*). Model simulations reproduce the latitudinal selectivity pattern of the extinction observed for the end-Permian (*16*).

We found that model similarity decreased as a function of grid cell distance and increased after the extinction, in qualitative agreement with the fossil analysis. However, absolute similarity values are larger in the model than the fossil record (Fig. 4). To facilitate a more direct correspondence between model simulations and the fossil record, we also restricted similarity analyses to only those locations represented in the fossil record using the grid cell centers of the fossil analysis grid ($n = 16$). This analysis leads to a similarity versus distance relationship with a higher signal-to-noise ratio than the global shelf relationship but does not qualitatively alter the initial similarity magnitude, decline with distance, or change in similarity simulated across the extinction (fig. S6). Instead, because the fossil record represents only a sample of the actual paleocommunity that lived at any given time, while model communities are perfectly sampled, this sampling difference has the potential to influence the model-data similarity comparison. We accounted for imperfect sampling of the fossil record in the model by randomly sampling a fraction of ecophysiotypes in each grid location in the similarity calculation. We tested a range of sampling fractions (25 to 100%) and found that a value of 40% visually reproduced the fossil record similarity magnitude and its change across the extinction both when similarity is computed for all shelf locations (Fig. 4) and when restricting the analysis to the locations of the fossil data (fig. S7).

Supplementary Materials

This PDF file includes:

Figs. S1 to S16

REFERENCES AND NOTES

1. D. M. Raup, J. J. Sepkoski Jr., Mass extinctions in the marine fossil record. *Science* **215,** 1501–1503 (1982).
2. S.-Z. Shen, J. L. Crowley, Y. Wang, S. A. Bowring, D. H. Erwin, P. M. Sadler, C.-Q. Cao, D. H. Rothman, C. M. Henderson, J. Ramezani, H. Zhang, Y. Shen, X.-D. Wang, W. Wang, L. Mu, W.-Z. Li, Y.-G. Tang, X.-L. Liu, L.-J. Liu, Y. Zeng, Y.-F. Jiang, Y.-G. Jin, Calibrating the end-Permian mass extinction. *Science* **334**, 1367–1372 (2011).
3. Á. T. Kocsis, C. J. Reddin, W. Kiessling, The biogeographical imprint of mass extinctions. *Proc. Biol. Sci.* **285**, 20180232 (2018).
4. E. Petsios, D. Bottjer, Quantitative analysis of the ecological dominance of benthic disaster taxa in the aftermath of the end-Permian mass extinction. *Paleobiology* **42**, 380–393 (2016).
5. W. J. Foster, K. Heindel, S. Richoz, J. Gliwa, D. J. Lehrmann, A. Baud, T. Kola-Jukovšek, D. Aljinović, B. Jurkovšek, D. Korn, R. C. Martindale, J. Peckmann, Suppressed competitive exclusion enabled the proliferation of Permian/Triassic boundary microbialites. *Depos. Rec.* **6**, 62–74 (2020).
6. D. J. Button, G. T. Lloyd, M. D. Ezcurra, R. J. Butler, Mass extinctions drove increased global faunal cosmopolitanism on the supercontinent Pangaea. *Nat. Commun.* **8**, 733 (2017).
7. S. Sahney, M. J. Benton, Recovery from the most profound mass extinction of all time. *Proc. Biol. Sci.* **275**, 759–765 (2008).
8. Z. T. Kulik, J. K. Lungmus, K. D. Angielczyk, C. A. Sidor, Living fast in the Triassic: New data on life history in *Lystrosaurus* (Therapsida: Dicynodontia) from northeastern Pangea. *PLOS ONE* **16**, e0259369 (2021).
9. C. A. Sidor, D. A. Vilhena, K. D. Angielczyk, A. K. Huttenlocker, S. J. Nesbitt, B. R. Peecook, J. S. Steyer, R. M. H. Smith, L. A. Tsuji, Provincialization of terrestrial faunas following the end-Permian mass extinction. *Proc. Natl. Acad. Sci. U.S.A.* **110**, 8129–8133 (2013).
10. X. Dai, H. Song, Toward an understanding of cosmopolitanism in deep time: A case study of ammonoids from the middle Permian to the Middle Triassic. *Paleobiology* **46**, 533–549 (2020).
11. S.-H. Zhang, S.-H. Shen, D. H. Erwin, Two cosmopolitanism events driven by different extreme paleoclimate regimes. *Glob. Planet. Change* **216**, 103899 (2022).
12. J. Yan, H. Song, X. Dai, Increased bivalve cosmopolitanism during the mid-Phanerozoic mass extinctions. *Palaeogeogr. Palaeoclimatol. Palaeoecol.* **611**, 110362 (2023).
13. J. D. Olden, N. L. Poff, Toward a mechanistic understanding and prediction of biotic homogenization. *Am. Nat.* **162**, 442–460 (2003).
14. C. L. Belanger, D. Jablonski, K. Roy, S. K. Berke, A. Z. Krug, J. W. Valentine, Global environmental predictors of benthic marine biogeographic structure. *Proc. Natl. Acad. Sci. U.S.A.* **109**, 14046–14051 (2012).
15. A. I. Miller, D. P. Buick, K. V. Bulinski, C. A. Ferguson, A. J. W. Hendy, M. Aberhan, W. Kiessling, Phanerozoic trends in the global geographic disparity of marine biotas. *Paleobiology* **35**, 612–630 (2009).
16. J. L. Penn, C. Deutsch, J. L. Payne, E. A. Sperling, Temperature-dependent hypoxia explains biogeography and severity of end-Permian marine mass extinction. *Science* **362**, eaat1327 (2018).
17. M. M. Joachimski, X. Lai, S. Shen, H. Jiang, G. Luo, B. Chen, J. Chen, Y. Sun, Climate warming in the latest Permian and the Permian–Triassic mass extinction. *Geology* **40**, 195–198 (2012).
18. K. V. Lau, K. Maher, D. Altiner, B. M. Kelley, L. R. Kump, D. J. Lehrmann, J. C. Silva-Tamayo, K. L. Weaver, M. Yu, J. L. Payne, Marine anoxia and delayed Earth system recovery after the end-Permian extinction. *Proc. Natl. Acad. Sci. U.S.A.* **113**, 2360–2365 (2016).
19. J. M. Sunday, A. E. Bates, N. K. Dulvy, Global analysis of thermal tolerance and latitude in ectotherms. *Proc. Biol. Sci.* **278**, 1823–1830 (2011).
20. J. L. Penn, C. Deutsch, Avoiding ocean mass extinction from climate warming. *Science* **376**, 524–526 (2022).
21. C. Deutsch, J. L. Penn, B. Seibel, Metabolic trait diversity shapes marine biogeography. *Nature* **585**, 557–562 (2020).
22. E. M. Howard, J. L. Penn, H. Frenzel, B. E. Seibel, D. Bianchi, L. Renault, F. Kessouri, M. A. Sutula, J. C. McWilliams, C. Deutsch, Climate-driven aerobic habitat loss in the California Current System. *Sci. Adv.* **6**, eaay3188 (2020).
23. C. J. Reddin, M. Aberhan, N. B. Raja, Á. T. Kocsis, Global warming generates predictable extinctions of warm- and cold-water marine benthic invertebrates via thermal habitat loss. *Glob. Change Biol.* **28**, 5793–5807 (2019).
24. B. J. Allen, M. E. Clapham, E. E. Saupe, P. B. Wignall, D. J. Hill, A. M. Dunhill, Estimating spatial variation in origination and extinction in deep time: A case study using the Permian–Triassic marine invertebrate fossil record. *Paleobiology* **49**, 509–526 (2023).
25. H. Song, P. B. Wignall, J. Tong, H. Yin, Two pulses of extinction during the Permian–Triassic crisis. *Nat. Geosci.* **6**, 52–56 (2013).
26. H. Song, S. Huang, E. Jia, X. Dai, P. B. Wignall, A. M. Dunhill, Flat latitudinal diversity gradient caused by the Permian-Triassic mass extinction. *Proc. Natl. Acad. Sci. U.S.A.* **117**, 17578–17583 (2020).
27. M. Foote, J. J. Sepkoski Jr., Absolute measures of the completeness of the fossil record. *Nature* **398**, 415–417 (1999).
28. J. Valentine, D. Jablonski, S. Kidwell, K. Roy, Assessing the fidelity of the fossil record by using marine bivalves. *Proc. Natl. Acad. Sci. U.S.A.* **103**, 6599–6604 (2006).
29. C. Deutsch, J. L. Penn, N. Lucey, Climate, oxygen, and the future of marine biodiversity. *Ann. Rev. Mar. Sci.* **16**, 217–245 (2024).
30. J. L. Penn, C. Deutsch, Geographical and taxonomic patterns in aerobic traits of marine ectotherms. *Philos. Trans. R. Soc. B* **379**, 20220487 (2024).
31. C. Deutsch, A. Ferrel, B. Seibel, H.-O. Pörtner, R. B. Huey, Climate change tightens a metabolic constraint on marine habitats. *Science* **348**, 1132–1135 (2015).
32. D. L. Rodland, D. J. Bottjer, Biotic recovery from the end-Permian mass extinction: Behavior of the inarticulate brachiopod *Lingula* as a disaster taxon. *Palaios* **16**, 95–101 (2001).
33. D. H. Erwin, The end and the beginning: Recoveries from mass extinctions. *Trends Ecol. Evol.* **13**, 344–349 (1998).
34. A. H. Knoll, R. K. Bambach, D. E. Canfield, J. P. Grotzinger, Comparative Earth history and Late Permian mass extinction. *Science* **273**, 452–457 (1996).
35. M. L. Fraiser, D. J. Bottjer, When bivalves took over the world. *Paleobiology* **33**, 397–413 (2007).
36. A. H. Knoll, R. K. Bambach, J. L. Payne, S. Pruss, W. W. Fischer, Paleophysiology and end-Permian mass extinction. *Earth Planet. Sci. Lett.* **256**, 295–313 (2007).
37. R. Plotnick, P. Wagner, Round up the usual suspects: Common genera in the fossil record and the nature of wastebasket taxa. *Paleobiology* **32**, 126–146 (2006).
38. H. Song, J. Tong, P. B. Wignall, M. Luo, L. Tian, H. Song, Y. Huang, D. Chu, Early Triassic disaster and opportunistic foraminifers in South China. *Geol. Mag.* **153**, 298–315 (2016).
39. J. K. Schubert, D. J. Bottjer, Aftermath of the Permian-Triassic mass extinction event: Paleoecology of Lower Triassic carbonates in the western USA. *Palaeogeogr. Palaeoclimatol. Palaeoecol.* **116**, 1–39 (1994).
40. W. J. Foster, R. J. Twitchett, Functional diversity of marine ecosystems after the Late Permian mass extinction event. *Nat. Geosci.* **7**, 233–238 (2014).
41. J. L. Payne, D. J. Lehrmann, J. Wei, M. J. Orchard, D. P. Schrag, A. H. Knoll, Large perturbations of the carbon cycle during recovery from the end-Permian extinction. *Science* **305**, 506–509 (2004).
42. Y. Sun, M. M. Joachimski, P. B. Wignall, C. Yan, Y. Chen, H. Jiang, L. Wang, X. Lai, Lethally hot temperatures during the Early Triassic greenhouse. *Science* **338**, 366–370 (2012).
43. N. Goudemand, C. Romano, M. Leu, H. Bucher, J. A. Trotter, I. S. Williams, Dynamic interplay between climate and marine biodiversity upheavals during the early Triassic Smithian-Spathian biotic crisis. *Earth Sci. Rev.* **195**, 169–178 (2019).
44. D. Altıner, J. L. Payne, D. J. Lehrmann, S. Özkan-Altıner, B. M. Kelley, M. M. Summers, M. Yu, Triassic Foraminifera from the Great Bank of Guizhou, Nanpanjiang Basin, South China: Taxonomic account, biostratigraphy, and implications for recovery from end-Permian mass extinction. *J. Paleo.* **95**, 1–53 (2021).
45. Y. Huang, Z.-Q. Chen, P. D. Roopnarine, M. J. Benton, L. Zhao, X. Feng, Z. Li, The stability and collapse of marine ecosystems during the Permian-Triassic mass extinction. *Curr. Biol.* **33**, 1059–1070.e4 (2023).
46. R. V. Solé, J. Saldaña, J. M. Montoya, D. H. Erwin, Simple model of recovery dynamics after mass extinction. *J. Theor. Biol.* **267**, 193–200 (2010).
47. P. M. Monarrez, N. A. Heim, J. L. Payne, Reduced strength and increased variability of extinction selectivity during mass extinctions. *R. Soc. Open Sci.* **10**, 230795 (2023).
48. E. K. Schaal, M. E. Clapham, B. L. Rego, S. C. Wang, J. L. Payne, Comparative size evolution of marine clades from the Late Permian through Middle Triassic. *Paleobiology* **42**, 127–142 (2016).
49. J. L. Payne, A. B. Jost, S. C. Wang, J. M. Skotheim, A shift in the long-term mode of foraminiferan size evolution caused by the end-Permian mass extinction. *Evolution* **67**, 816–827 (2013).
50. B. L. Rego, S. C. Wang, D. Altiner, J. L. Payne, Within- and among-genus components of size evolution during mass extinction, recovery, and background intervals: A case study of Late Permian through Late Triassic foraminifera. *Paleobiology* **38**, 627–643 (2012).
51. W. J. Foster, J. Gliwa, C. Lembke, A. C. Pugh, R. Hofmann, M. Tietje, S. Varela, L. C. Foster, D. Korn, M. Aberhan, Evolutionary and ecophenotypic controls on bivalve body size distributions following the end-Permian mass extinction. *Global Planet. Change* **185,** 103088 (2020).
52. J. L. Payne, Evolutionary dynamics of gastropod size across the end-Permian extinction and through the Triassic recovery interval. *Paleobiology* **31**, 269–290 (2005).
53. A. Brayard, L. J. Krumenacker, J. P. Botting, J. F. Jenks, K. G. Bylund, E. Fara, E. Vennin, N. Olivier, N. Goudemand, T. Saucède, S. Charbonnier, C. Romano, L. Doguzhaeva, B. Thuy, M. Hautmann, D. A. Stephen, C. Thomazo, G. Escarguel, Unexpected Early Triassic marine ecosystem and the rise of the Modern evolutionary fauna. *Sci. Adv.* **3**, e1602159 (2017).

54. W. J. Foster, G. Asatryan, S. Rauzi, J. P. Botting, S. Z. Buchwald, D. B. Lazarus, T. Isson, J. Renaudie, W. Kiessling, Response of siliceous marine organisms to the Permian-Triassic climate crisis based on new findings from central Spitsbergen, Svalbard. *Paleoceanogr. Paleoclimatol.* **38**, e2023PA004766 (2023).
55. R. Hofmann, M. Hautmann, H. Bucher, Recovery dynamics of benthic marine communities from the Lower Triassic Werfen Formation, northern Italy. *Lethaia* **48**, 474–496 (2015).
56. J. L. Payne, D. J. Lehrmann, J. Wei, A. H. Knoll, The pattern and timing of biotic recovery from the end-Permian extinction on the Great Bank of Guizhou, Guizhou Province, China. *Palaios* **21**, 63–85 (2006).
57. M. Foote, A. I. Miller, Determinants of early survival in marine animal genera. *Paleobiology* **39**, 171–192 (2013).
58. M. L. McKinney, J. L. Lockwood, Biotic homogenization: A few winners replacing many losers in the next mass extinction. *Trends Ecol. Evol.* **14**, 450–453 (1999).
59. M. L. McKinney, J. L. Lockwood, "Biotic homogenization: A sequential and selective process" in *Biotic Homogenization*, M. L. McKinney, J. L. Lockwood, Eds. (Kluwer/Plenum, 2001), pp. 1–18.
60. A. Ziska, D. Silvestro, T. Andermann, J. Azevedo, C. Ritter, S. Svanteson, N. Wengstrom, V. Ziska, A. Antonelli, CoordinateCleaner: Standardized cleaning of occurrence records from biological collection databases. *Methods Ecol. Evol.* **7**, 1303–1310 (2019).
61. J. T. Flannery-Sutherland, N. B. Raja, Á. T. Kocsis, W. Kiessling, *Fossilbrush*: An R package for automated detection and resolution of anomalies in paleontological occurrence data. *Methods Ecol. Evol.* **13**, 2171–2183 (2022).
62. Á. T. Kocsis, icosa: Global triangular and penta-hexagonal grids based on tessellated icosahedra, R package version 0.11.0 (2023); https://adamkocsis.github.io/icosa/.
63. C. R. Scotese, *PALEOMAP PaleoAtlas for GPlates and the PaleoDataPlotter Program,* Tutor, PALEOMAP Project (2016); www.earthbyte.org/paleomap-paleoatlas-for-gplates/.
64. R. D. Müller, J. Cannon, X. Qin, R. J. Watson, M. Gurnis, S. Williams, T. Pfaffelmoser, M. Seton, S. H. J. Russell, S. Zahirovic, GPlates: Building a virtual Earth through deep time. *Geochem. Geophys. Geosyst.* **19**, 2243–2261 (2018).
65. Á. T. Kocsis, N. B. Raja, S. D. Williams, Rgplates: R interface for the GPlates Web Service and Desktop Application (2024); https://adamtkocsis.com/rgplates/.

Acknowledgments: We thank K. Boyce and E. Sperling for the many stimulating conversations regarding the manuscript. We thank Á. Kocsis for continuous discussions and advice regarding using the *icosa* R Package. We are grateful to the many contributors to the Paleobiology Database whose contributions made this research possible. **Funding:** This work was supported by National Science Foundation grant EAR-2121392 (to J.L.Pa.), National Science Foundation grant EAR-2121466 (to C.D.), Saudi Arabian Cultural Mission Graduate Fellowship (to J.A.A.), Stanford University Graduate Research Assistantship (to J.A.A.), the Wallenberg Foundation Postdoctoral Scholarship KAW 2022.0330 (to M.B.), and Princeton University and Geophysical Fluid Dynamics Laboratory (GFDL)'s Cooperative Institute for Modeling the Earth System (CIMES) (to J.L.Pe.). **Author contributions:** Conceptualization: J.A.A., J.L.Pe., M.B., C.D., and J.L.Pa. Methodology: J.A.A., J.L.Pe., P.M.M., M.B., C.D., and J.L.Pa. Software: J.A.A., J.L.Pe., M.B., P.M.M., C.D., and J.L.Pa. Validation: J.A.A., J.L.Pe., and M.B.. Formal analysis: J.A.A., J.L.Pe., P.M.M., M.B., and J.L.Pa. Investigation: J.A.A., J.L.Pe., M.B., and J.L.Pa. Resources: J.A.A., J.L.Pe., and M.B. Data curation: J.A.A., J.L.Pe., and M.B. Visualization: J.A.A., J.L.Pe., and M.B. Funding acquisition: C.D. and J.L.Pa. Project administration: C.D. and J.L.Pa. Supervision: C.D. and J.L.Pa. Writing—original draft: J.A.A., J.L.Pe., M.B., and J.L.Pa. Writing—review and editing: J.A.A., J.L.Pe., M.B., and J.L.Pa. **Competing interests:** The authors declare that they have no competing interests. **Data and materials availability:** All data, code, and materials used in the analysis are available in zenodo.org/doi/10.5281/zenodo.11522106. All other data needed to evaluate the conclusions in this paper are present in the paper and/or the Supplementary Materials.

Submitted 29 June 2024
Accepted 24 February 2025
Published 26 March 2025
10.1126/sciadv.adr4199